光学学报

原子喷泉中基于电光调制的激光移频与稳频

赵伟靖[1,2]，李耀[1,2]，董日昌[3]，魏荣[1,2*]

[1]中国科学院上海光学精密机械研究所量子光学重点实验室，上海 201800；
[2]中国科学院大学，北京 100049；
[3]中国科学院微小卫星创新研究院，上海 200120

摘要 激光稳频是影响原子喷泉系统性能的关键技术。提出了一种应用于原子喷泉系统的激光稳频优化方案。该方案将激光冷却过程中采用的移频方法应用到稳频系统中，通过光纤电光调制的方法产生边带，并将频率锁定在边带的饱和吸收峰上。同时应用大光斑饱和吸收模块，改善饱和吸收信号和误差信号的信噪比。利用 ^{85}Rb 原子喷泉系统主光路的探测光，通过 1.035 GHz 的移频，实现从 ^{85}Rb 饱和吸收峰到 ^{87}Rb 饱和吸收峰的转移锁定，并在 ^{85}Rb 喷泉系统中观测到冷原子云信号。锁定后的信号可实现较长时间的稳定工作。该方案通过控制电光调制频率，还有望实现激光冷却实验范围内的任意频率锁定，具有重要的应用价值。

关键词 原子喷泉；电光调制；移频；饱和吸收；稳定度

中图分类号 O562.2 **文献标志码** A **DOI**：10.3788/AOS230611

1 引 言

原子频标[1-2]近年来取得了飞速发展。其中喷泉频标的精度已经达到了 10^{-16}[3]，目前已经作为一级[3-6]和二级频标[4-5]在复现秒定义和国际原子时（TAI）[6]方面发挥着主导性的作用。而光频标作为目前精度最高的原子频标，不确定度已经达到了 10^{-19}[7-10]，有望取代Cs原子成为新的秒定义[11]。原子频标的发展离不开激光器[12-13]与激光稳频技术[1，14-16]的进步。无论是原子离子的俘获、冷却，还是光子的囚禁，基于激光稳频技术的窄线宽、超窄线宽激光都发挥了非常重要的作用。

目前常用的稳频方法包括利用原子的饱和吸收性质进行饱和吸收峰锁定的饱和吸收谱稳频[17-18]、利用调制将调制光束转移到反向未调制光束从而产生四波混频的调制转移光谱稳频[19-21]和利用调制器件将输入激光进行调制解调从而将激光频率稳定到光学谐振腔的PDH（Pound-Drever-Hall）稳频[22-24]等等。饱和吸收技术[1，15]因其操作简单、分辨率高且可消除多普勒加宽等特点，广泛应用在原子频标的稳频领域，是微波波段的原子喷泉钟普遍采用的技术。喷泉钟的激光稳频是将激光频率锁定于特定的饱和吸收峰上实现的，一般情况下，应用于激光稳频的原子饱和吸收谱线包含多个饱和吸收峰。考虑到后续要实现冷原子实验需要的俘获、冷却、上抛等功能，还需对稳频后的激光频率进行相应的调制、移频。因此参与稳频的饱和吸收峰一般位置固定，使得谱线的其他峰无法实现应用。

本文提出了一种激光稳频的优化方案。该方案通过光纤电光调制的方法对稳频激光进行移频调制，从而实现了不同饱和吸收跃迁峰之间的转移锁定。同时为了进一步提高饱和吸收谱线的信噪比（SNR），采用了大光斑饱和吸收光路。通过增大通光孔径的方法，优化激光稳频信号。在 ^{85}Rb[25]喷泉钟上进行了实验验证，通过 1.035 GHz 的大范围移频，将一级边带调谐到 ^{87}Rb 原子的饱和吸收共振峰上并实现稳定锁定。通过电光调制，还有望进一步利用时序控制实现快速移频来替代喷泉主光路中部分声光调制器的作用，从而简化喷泉钟主光路，使系统更加可靠、稳定。

2 实验原理及设计

铷原子喷泉系统中稳频的参考信号是铷原子的饱和吸收谱线。本文中实现稳频的过程首先是将输入激光通过电光调制进行移频，然后将移频后的激光输入饱和吸收模块进行饱和吸收光谱信号探测，接着将光谱信号进行调制解调从而产生误差信号，最后根据误差信号产生特定反馈信号从而控制激光器的输出频率。对于电场强度 $E=E_0\mathrm{e}^{\mathrm{j}\nu_0 t}$ 的输入激光，通过电光调制器进行相位调制后的电场强度表示为

$$E=E_0\mathrm{e}^{\mathrm{j}\nu_0 t}\mathrm{e}^{\mathrm{j}\alpha\sin(\nu_\mathrm{m} t)},\tag{1}$$

收稿日期：2023-03-01；**修回日期**：2023-04-13；**录用日期**：2023-04-26；**网络首发日期**：2023-05-08

基金项目：中国科学院战略性先导科技专项（B类）（XDB21030200）、国家重点研发计划（2021YFA0718303）

通信作者：*weirong@siom.ac.cn

式中：υ_0表示激光共振频率；α表示调制深度；υ_m表示调制频率。由于$\mathrm{e}^{\mathrm{j}\alpha\sin(\upsilon_\mathrm{m}t)}$项满足贝塞尔函数，因此式（1）可化简为

$$E(t)=E_0\mathrm{e}^{\mathrm{j}\upsilon_0 t}[\mathrm{J}_0(\alpha)+2\mathrm{j}\mathrm{J}_1(\alpha)\sin(\upsilon_\mathrm{m}t)+2\mathrm{J}_2(\alpha)\sin(2\upsilon_\mathrm{m}t)+2\mathrm{j}\mathrm{J}_3(\alpha)\sin(3\upsilon_\mathrm{m}t)+\cdots],\quad(2)$$

式（2）括号中的各项即表示通过电光调制引入的各级边带。考虑到0级衍射光无法满足移频的需求，喷泉系统一般取+1（或者−1）级衍射光作为有效激光。因此，在激光输入饱和吸收模块之前，需要通过调节调制深度来实现1级边带功率最大。已知光强$I=\sqrt{E\cdot E^*}$，结合式（2）可知，当应用电光调制器进行相位调制时，输入总光强I_0会随着调制深度的改变不同程度地分布在各调制边带上，且均小于I_0。因此经过调制后的激光输出的信号必然小于未调制前的信号。为了解决信号变小的问题，本文采用了大光斑饱和吸收的方案。对于一个二能级系统，饱和吸收[1]表示为

$$V_\mathrm{sat}=\frac{S_0}{2(1+S_0)}\cdot\frac{1}{1+\left[(2\delta\nu)/\gamma'\right]^2},\quad(3)$$

式中：$S_0=I/I_\mathrm{sat}$表示共振饱和参量，其中I表示输入光强，I_sat表示饱和吸收光强；$\delta\nu$表示频率失谐量；$\gamma'=\gamma\sqrt{1+S_0}$为饱和展宽后的线宽，其中$\gamma$表示原子的自然线宽，整个谱线的线型满足洛伦兹（Lorentz）线型。对于^{85}Rb原子，饱和吸收光强为1.6 mW/cm^2，自然线宽为6 MHz[15]。由式（3）可知，当S_0增大时，饱和吸收信号会随之增大。因此通过移频以及大光斑饱和吸收的双向结合，则可实现较强的移频信号输出。

实验装置如图1（a）所示，该装置由两大模块组成，移频模块和饱和吸收模块。移频模块用于实现频率转移，饱和吸收模块用于产生及放大饱和吸收信号，提高信号SNR。移频模块是由光纤电光调制器（FEOM）及其控制器件构成的，包括射频控制器（ADF4351）及放大器。该射频控制器通过调节输出频率以及功率来控制移频量以及边带特征。饱和吸收模块是自主搭建的一套饱和吸收光路系统，其实物图如图1（b）所示。该模块最大的特点在于应用了大口径输出光斑的光纤准直器以及用于控制注入光路光斑直径的可调光阑（最大孔径约10 mm），其目的就是通过增大通光孔径来增强激光与铷泡中铷原子的作用范围，从而提高饱和吸收跃迁概率信号，进而提高SNR。

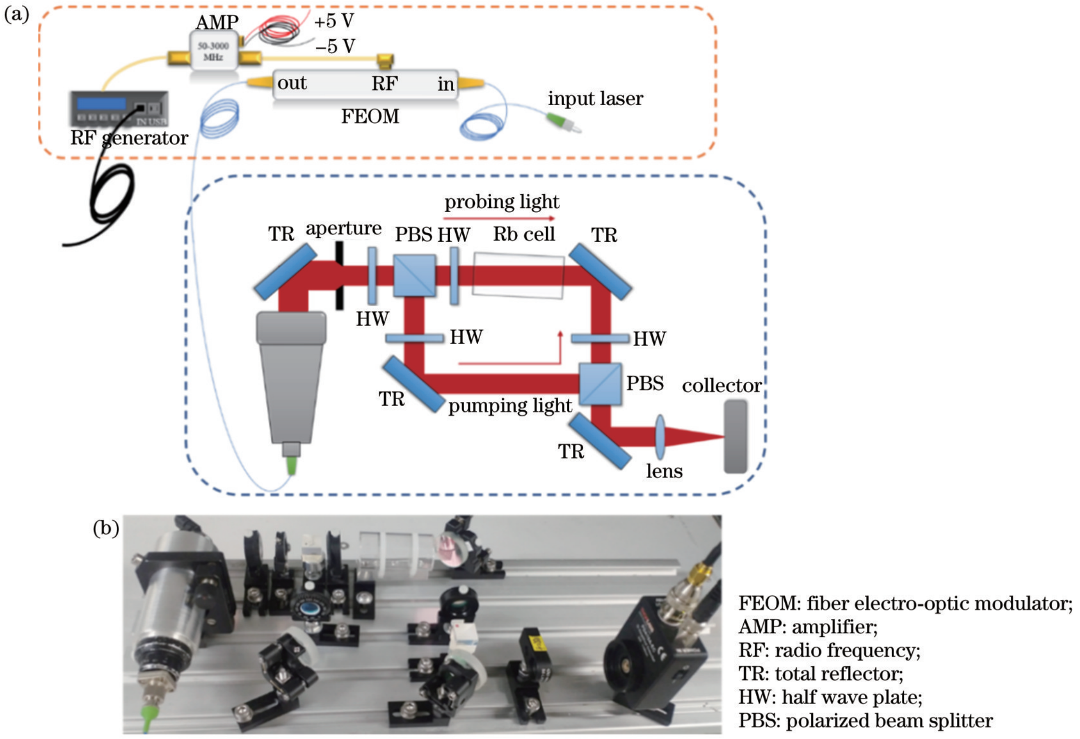

FEOM: fiber electro-optic modulator;
AMP: amplifier;
RF: radio frequency;
TR: total reflector;
HW: half wave plate;
PBS: polarized beam splitter

图1 实验装置。（a）移频实验装置原理图；（b）大孔径饱和吸收光路实物图

Fig. 1 Experimental setup. (a) Schematic diagram of frequency shift device; (b) physical image of large aperture saturated absorption optical path

实验整体的能级转移过程如图2所示。为了较清晰地说明能级变化情况，在绘图过程中对实际能级对应位置及比例进行了部分修改，将两原子基态高能级位置进行对齐且将激发态相对于基态的比例进行了部分放大，从而更清晰地说明激发态精细结构的变化，实际能级结构并非如此。整体的实验设计是利用^{85}Rb原子钟主光路的探测光将^{85}Rb原子的$|F=3\rangle\rightarrow|F'=3\rangle\otimes|F'=4\rangle$共振跃迁峰移频到^{87}Rb

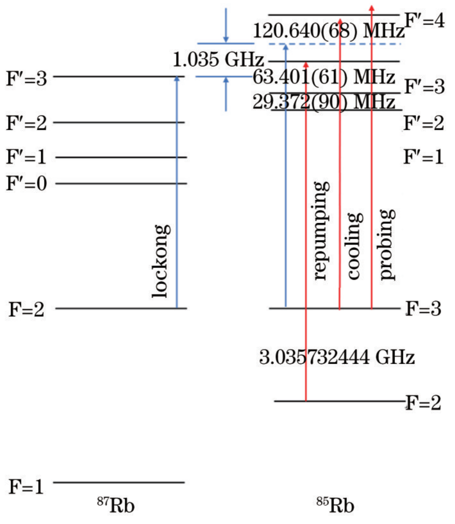

图 2　能级转移图

Fig. 2　Energy level transfer diagram

原子的$|F=2\rangle \rightarrow |F'=3\rangle$共振跃迁峰并实现锁定。^{85}Rb 原子的$|F=3\rangle \rightarrow |F'=3\rangle \otimes |F'=4\rangle$共振跃迁频率对应于^{85}Rb 喷泉系统的锁频点，为实现 GHz 量级的移频，将频率移至移频量级较大的^{87}Rb 原子的共振跃迁峰上。本文实验以移频至^{87}Rb 原子的$|F=2\rangle \rightarrow |F'=3\rangle$跃迁峰为例，整个过程共移频 1.035 GHz。应用主光路的光作为光源是考虑到主光路性能稳定，有利于实现信号稳定输出。

3　实验验证及结果分析

实验的第一步是实现对 FEOM 产生的边带位置及功率分布的调控，边带位置是根据具体的移频要求通过精细结构能级跃迁计算所得，本实验共需要移频 1.035 GHz。而对于所产生边带功率分布的调控，相对比较复杂，需通过改变调制深度来调节边带的强弱。这个过程本文是通过法布里-珀罗(F-P)干涉仪来实现的。将调制的激光输入到 F-P 干涉仪中，通过示波器进行数据监测，测量得 FEOM 边带随微波功率变化结果如图 3 所示。曲线 0～3 分别表示 FEOM 的 0～3 级边带随微波功率的变化，曲线 J_0～J_3表示贝塞尔函数 0～3 级边带随微波功率的变化情况，FEOM 边带变化满足贝塞尔函数，与式(2)相呼应。选取 1 级功率最大且其他级功率尽可能小的位置对应的边带作为调制边带，对应的微波功率约为 14 dBm，此时 1 级边带的功率占比约为总功率的 34%，调制后的输出信号减小。

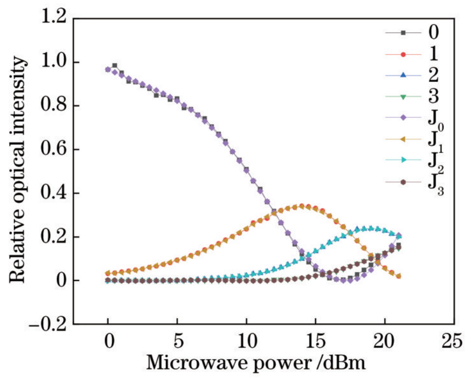

图 3　FEOM 各级调制输出与功率的关系

Fig. 3　Relationship between modulation output and power of each level of FEOM

为进一步增大调制后的信号，应用大光斑饱和吸收模块进行饱和吸收，如图 1(b)所示。从光纤准直器出射的光经过第一个偏振分光棱镜(PBS)分成两束，透射光作为探测光通过铷泡，反射光作为泵浦光经过第二个 PBS 反射后通过铷泡，生成的饱和吸收信号经过透镜会聚到收集器进行信号探测。铷泡通光口径约 25 mm，长约 50 mm。探测光与泵浦光的比例为 1∶2，各路光的分光均通过调节半波片进行控制。一般的饱和吸收模块应用的是小光斑激光，直径约为 2 mm，而本文使用的模块的激光直径可达 10 mm，且可根据需求的不同改变光阑的通光孔径。为比较大、小光斑直径对饱和吸收信号的影响，本文进行了大量的实验验证。图 4 表示将移频后的激光馈入到大孔径饱和吸收模块后，不同光斑直径条件下观察到的饱和吸收谱线。图 4(a)和 4(b)是在输入总光功率不变(P=2 mW)的条件下得到的，图 4(a)表示饱和吸收跃迁谱线随光斑直径的变化。图 4(b)对应于饱和吸收谱线 SNR 随光斑直径的变化。由图 4 分析可知，随着光斑直径的增大，饱和吸收跃迁谱线信号逐步增强，SNR 逐步提高，与由式(3)得出的结论相呼应。同时观察到 SNR 的变化呈现出先快后满的增长趋势，造成该现象的原因可能是，在增大谱线信号的过程中，链路中的电学噪声被放大，影响了信号 SNR 的持续增长，因此本文实验中并未选择更大的光斑直径进行实验。当光斑直径从 2 mm 增大到 10 mm 时，谱线整体的 SNR 提高了约 13 dB。

图 4(c)和 4(d)表示饱和吸收误差信号与光斑直径之间的关系，是在不同输入光功率条件下得到的。图 4(c)列举了当光斑直径分别对应于 3 mm 和 8 mm 时，误差信号随输入光功率的变化。当输入光功率不变时，随着光斑直径增大，误差信号变大，斜率变大；当输入光功率不断增大时，误差信号增大，且大光斑条件下的变化更为明显。图 4(d)列举了多种光斑直径下，输入光功率与误差信号斜率之间的关系，说明增大光斑直径与增强输入光功率均对饱和吸收信号的提升产生正向的影响。综合图 4(a)～4(d)可得，光斑直径越大，输入光功率越大，得到的饱和吸收信号越强，SNR 越高。

将经过大光斑饱和吸收模块输出的不同情况下的饱和吸收信号进行比较，如图 5 所示。图 5(a)和 5(b)表示输入总光功率为 2 mW、光斑直径为 2 mm 时的情况，其中图 5(a)表示未经调制的饱和吸收信号，

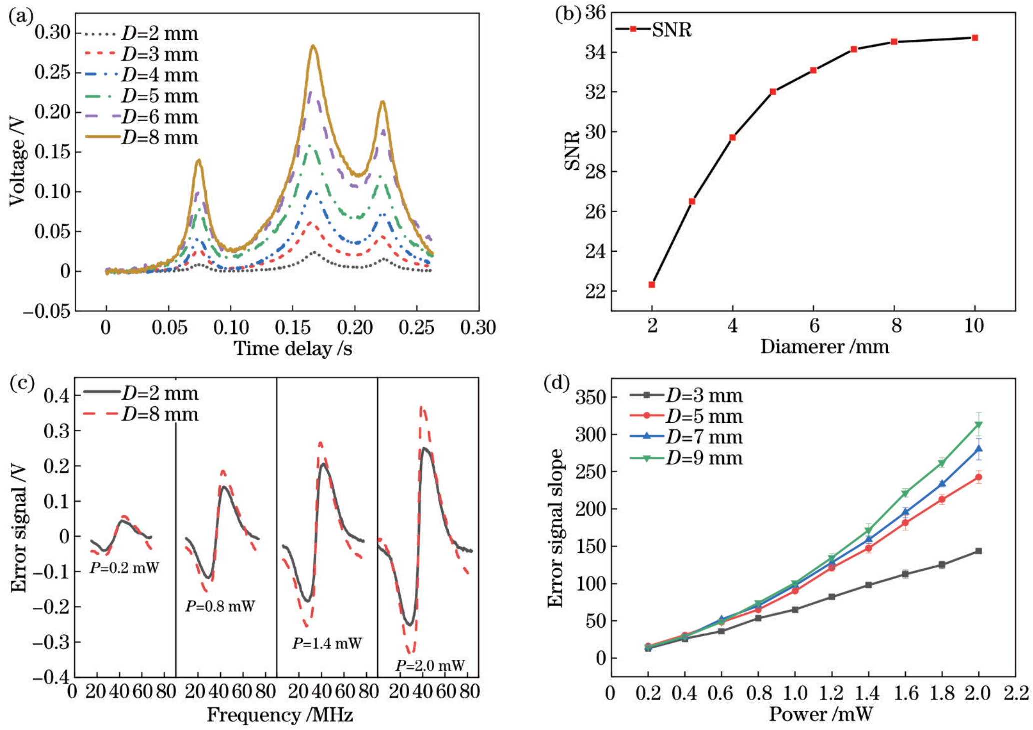

图4　饱和吸收信号与光斑直径的关系。(a) 跃迁信号随光斑直径的变化；(b) 饱和吸收信号条纹的SNR随光斑直径的变化；(c) 当光斑直径分别为3 mm和8 mm时，饱和吸收误差信号随光功率的变化；(d) 误差信号斜率随光功率变化

Fig. 4　Relationsheep between saturated absorption signal and spot diameter. (a) Changes of transition signal with spot diameter; (b) changes of SNR of saturated absorption signal stripe with spot diameter; (c) relationsheep between saturated absorption error signal and laser power when spot diameters are 3 mm and 8 mm, respectively; (d) changes of error signal slope with laser power

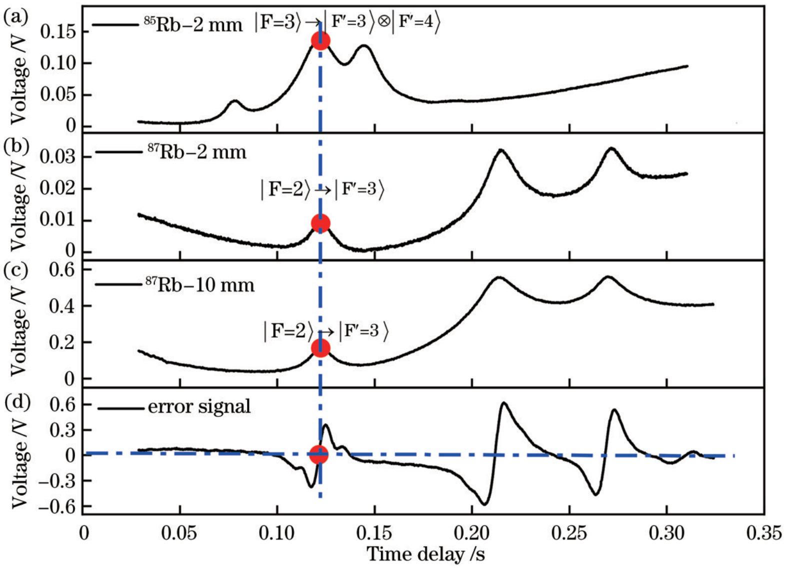

图5　调制前后的饱和吸收信号。(a) 调制前的信号；(b) 调制后的信号；(c) 调制后增大光斑直径的信号；(d) 调制后的误差信号

Fig. 5　Saturated absorption signals before and after modulation. (a) Signal before modulation; (b) signal after modulation; (c) signal with increased spot diameter after modulation; (d) error signal after modulation

图5(b)表示经过移频调制后得到的饱和吸收信号。由此可以分析出，经过电光调制移频后，^{85}Rb原子的$|F=3\rangle\rightarrow|F'=3\rangle\otimes|F'=4\rangle$跃迁峰移移频到了^{87}Rb原子的$|F=2\rangle\rightarrow|F'=3\rangle$跃迁峰，但信号幅度减小了约1/4，与前文中关于移频模块的分析结论一致。图5(c)和5(d)表示输入总光功率不变时，光斑直径为10 mm时得到的调制后的饱和吸收信号和误差信号。比较图5(b)和5(c)，当光斑直径从2 mm增大到10 mm时，饱和吸收信号增大了约20倍，SNR也有了明显的提高。将移频后在图5(b)和5(c)两种条件下

得到的 ^{87}Rb 原子的$|F=2\rangle\rightarrow|F'=3\rangle$饱和吸收跃迁峰分别进行锁定。由于图 5(b)对应的信号太小，无法实现对应峰值锁定，而图 5(c)则可实现锁定，且锁定后的信号在 ^{85}Rb 喷泉钟上成功捕获到了冷原子云信号，如图 6 所示。捕获的原子云是在磁光阱(MOT)区冷却后准备上抛的信号，由 CCD 监测所得。

对锁定后的稳频信号进行实时监测，结果如图 7 所示。图 7(a)表示误差信号中心位置随时间的变化，是分别对单次采集的误差信号进行处理得到的，中心位置整体起伏约 0.0005 V。图 7(a)中插图表示锁定后的误差信号，为单次监测的结果，信号的峰峰值约为 0.006 V。由此可知，信号的起伏相比于信号本身小了约一个数量级，约为信号的 8%。因此，整体的起伏变化对锁定后的信号稳定性的影响可以忽略。在整个监测过程中，系统一直处于连续锁定的状态。图 7(b)表示稳频过程中由喷泉钟系统探测到的下落原子数随时间的变化情况，原子数起伏约占整体信号的 17% 且变化情况比较稳定。因此，经过 FEOM 移频后并由大光斑饱和吸收模块放大的饱和吸收信号完全符合喷泉钟系统长期稳定运行的需求。

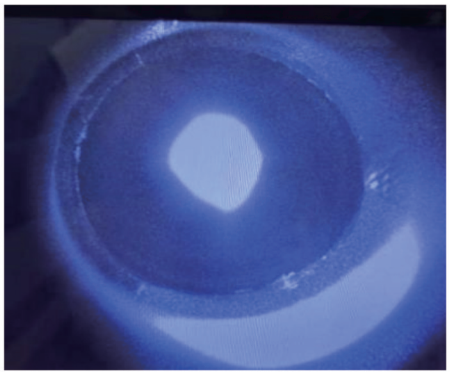

图 6　MOT 中心的冷原子云

Fig. 6　Cold atom cloud in MOT center

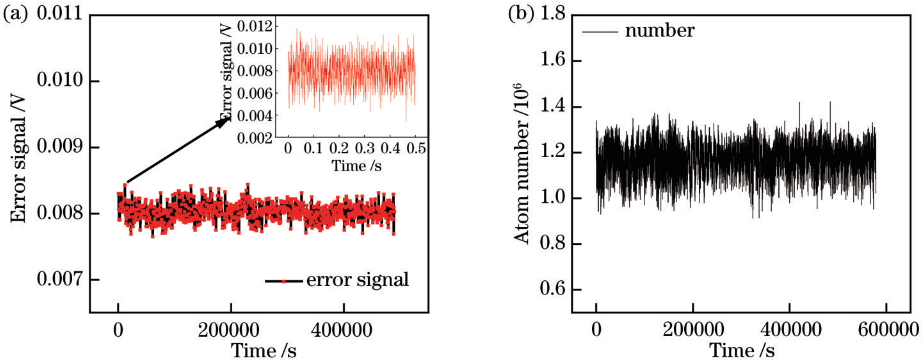

图 7　稳频过程中的信号随时间的变化。(a) 饱和吸收误差信号(插图为采集误差信号)(注：锁定后的误差信号略偏开 0 点附近是由于激光锁定控制系统增益较小，并不影响实验的正常运行)；(b)下落到探测区的原子数

Fig. 7　Change of signal with time during frequency stabilization. (a) Saturation absorption error signal (illustration: acquisition error signal) (Note: error signal after locking slightly deviates from 0 is due to small gain of laser locking control system, which does not affect normal operation of experiment); (b) number of atoms falling into detection zone

通过 FEOM 移频，实现了原子不同能级间的相互转移锁定，若将该方法与时序上的快速控制结合，则可应用到喷泉主光路系统中实现光路移频部分的进一步简化。为实现原子的冷却、探测等功能，本文作者课题组的 ^{87}Rb 原子喷泉钟[26]和 ^{85}Rb 原子喷泉钟[25]的主光路均包含多个移频器件且伴随着单个器件的多次移频，复杂且传输效率低[27]。图 8(a)为目前 ^{85}Rb 原子喷泉钟的主光路示意简图。如果可以实现时序上的快速移频控制，则可在输入激光前增加 FEOM，并根据主光路不同时间段内的移频需求对 FEOM 进行调控，从而实现主光路中的部分声光调制器(AOM)的功能，简化主光路，甚至实现激光传输效率高、光学系统鲁棒性高的全光纤链路，如图 8(b)所示。但目前这一想法本课题组并没有实现，这也是下一步要努力的方向。

4　结　论

本文提出了一种应用于原子喷泉系统的激光稳频的优化方案，通过电光调制对入射光进行移频，实现了用 ^{85}Rb 喷泉钟主光路中的探测光从 ^{85}Rb 共振交叉峰到 ^{87}Rb 跃迁峰 GHz 量级的转移锁定。通过增大饱和吸收通光孔径的方法，将得到的跃迁谱线 SNR 进行了优化，SNR 提高了约 13 dB。将跃迁铺线进行锁定，成功在原子喷泉钟上观察到了原子云并监测到了稳定的输出信号。通过这种优化方案，有望实现频率范围内的任一频率的转移锁定。还可以将移频的理念应用到主光路的优化中，减少主光路中调制器的数量，进一步简化光路，为全光纤链路的实现提供了可能。

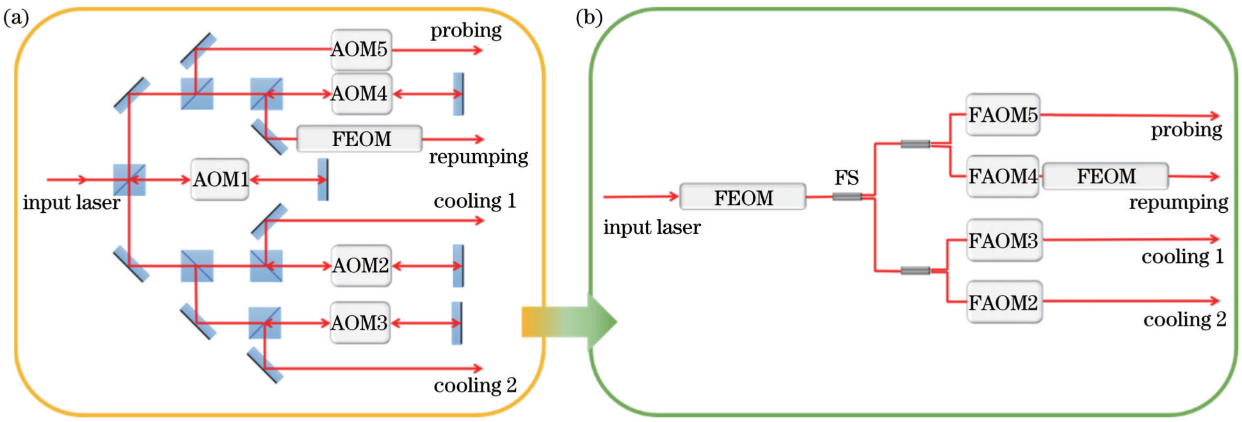

AOM: acousto-optic modulator; FAOM: fiber acousto-optic modulator, FS: fiber splitter

图 8 原子喷泉钟主光学链路。(a) 光路图；(b) 全光纤链路图

Fig. 8 Main optical link of atomic fountain clock. (a) Optical path; (b) all fiber link

参考文献

[1] Riehle F. Frequency standards: basic and applications[M]. Weinheim: WILEY-VCH Verlag GmbH & Co. KGaA, 2004.

[2] Audoin C, Vanier J. Atomic frequency standards and clocks[J]. Journal of Physics E: Scientific Instruments, 1976, 9(9): 697-720.

[3] Zhang H, Ruan J, Liu D D, et al. Development and preliminary operation of 87Rb continuously running atomic fountain clock at NTSC[J]. IEEE Transactions on Instrumentation and Measurement, 2022, 71: 1008312.

[4] Hachisu H, Petit G, Nakagawa F, et al. SI-traceable measurement of an optical frequency at the low 10^{-16} level without a local primary standard[J]. Optics Express, 2017, 25 (8): 8511-8523.

[5] Guéna J, Abgrall M, Clairon A, et al. Contributing to TAI with a secondary representation of the SI second[J]. Metrologia, 2014, 51(1): 108-120.

[6] BIPM Annual Report on Time Activities[EB/OL]. [2023-02-01]. https://webtai.bipm.org/ftp/pub/tai/annual-reports/bipm-annual-report/annual_report_2020.pdf.

[7] McGrew W F, Zhang X, Fasano R J, et al. Atomic clock performance enabling geodesy below the centimetre level[J]. Nature, 2018, 564(7734): 87-90.

[8] Huang Y, Zhang B L, Zeng M Y, et al. Liquid-nitrogen-cooled Ca^+ optical clock with systematic uncertainty of 3×10^{-18}[J]. Physical Review Applied, 2022, 17(3): 034041.

[9] Bothwell T, Kennedy C J, Aeppli A, et al. Resolving the gravitational redshift across a millimetre-scale atomic sample[J]. Nature, 2022, 602(7897): 420-424.

[10] 卢晓同, 常宏. 光晶格原子钟研究进展[J]. 光学学报, 2022, 42 (3): 0327004.
Lu X T, Chang H. Progress of optical lattice atomic clocks[J]. Acta Optica Sinica, 2022, 42(3): 0327004.

[11] Bize S. The unit of time: present and future directions[J]. Comptes Rendus Physique, 2019, 20(1/2): 153-168.

[12] Jin W, Yang Q F, Chang L, et al. Hertz-linewidth semiconductor lasers using CMOS-ready ultra-high-Q microresonators[J]. Nature Photonics, 2021, 15(5): 346-353.

[13] Fermann M E, Hartl I. Ultrafast fibre lasers[J]. Nature Photonics, 2013, 7(11): 868-874.

[14] Cartaleva S S, Gateva S V. Mode selection and frequency stabilization in lasers[J]. Progress in Quantum Electronics, 1994, 18(4): 275-375.

[15] Metcalf H J, Straten P V D. Laser cooling and trapping[M]. New York: Springer, 1999: 37-40.

[16] 吉经纬, 程鹤楠, 张镇, 等. 可搬运铷喷泉原子钟全自动激光稳频系统[J]. 光学学报, 2020, 40(22): 2214002.
Ji J W, Cheng H N, Zhang Z, et al. Automatic laser frequency stabilization system for transportable ^{87}Rb fountain clock[J]. Acta Optica Sinica, 2020, 40(22): 2214002.

[17] Chebotayev V. Supernarrow saturated absorption resonances[J]. Physics Reports, 1985, 119(2): 75-116.

[18] Brazhnikov D, Abdel Hafiz M, Coget G, et al. Ultrahigh-contrast saturated-absorption resonance to enhance stability of CPT atom clocks[C]//2017 Joint Conference of the European Frequency and Time Forum and IEEE International Frequency Control Symposium (EFTF/IFCS), July 9-13, 2017, Besancon, France. New York: IEEE Press, 2017: 278-281.

[19] 刘涛, 闫树斌, 李利平, 等. 铯原子调制转移光谱在激光稳频中的应用[J]. 光子学报, 2003, 32(1): 5-8.
Liu T, Yan S B, Li L P, et al. Frequency stabilization of laser diode via modulation transfer spectrum in cesium vapor cell[J]. Acta Photonica Sinica, 2003, 32(1): 5-8.

[20] Chen S Z, Liu Q, Shen Y, et al. Study on modulation transfer spectroscopy of Rb atoms[C]//2017 29th Chinese Control and Decision Conference (CCDC), May 28-30, 2017, Chongqing, China. New York: IEEE Press, 2017: 5830-5834.

[21] 洪毅, 侯霞, 陈迪俊, 等. 基于 Rb^{87}调制转移光谱稳频技术研究[J]. 中国激光, 2021, 48(21): 2101003.
Hong Y, Hou X, Chen D J, et al. Research on frequency stabilization technology of modulation transfer spectroscopy based on Rb^{87}[J]. Chinese Journal of Lasers, 2021, 48(21): 2101003.

[22] Black E D. An introduction to Pound—Drever—Hall laser frequency stabilization[J]. American Journal of Physics, 2001, 69 (1): 79-87.

[23] Idjadi M H, Aflatouni F. Integrated Pound—Drever—Hall laser stabilization system in silicon[J]. Nature Communications, 2017, 8: 1209.

[24] Gillot J, Tetsing-Talla S F, Denis S, et al. Digital control of residual amplitude modulation at the 10^{-7} level for ultra-stable lasers[J]. Optics Express, 2022, 30(20): 35179-35188.

[25] Wang Q A, Zhang N, Guang W, et al. Precision measurements of the ground-state hyperfine splitting of ^{85}Rb using an atomic fountain clock[J]. Physical Review A, 2019, 100(2): 022510.

[26] Du Y B, Wei R, Dong R C, et al. Recent improvements on the atomic fountain clock at SIOM[J]. Chinese Physics B, 2015, 24 (7): 070601.

[27] 姬清晨, 董日昌, 王倩, 等. 基于型材网格平台的紧凑 ^{85}Rb 喷泉钟光路设计[J]. 光学学报, 2020, 40(18): 1802001.

Ji Q C, Dong R C, Wang Q, et al. Design of compact ^{85}Rb fountain optical path based on profile gridded platform[J]. Acta Optica Sinica, 2020, 40(18): 1802001.

Laser Frequency Shift and Stabilization of Atomic Fountain Based on Electro-Optic Modulation

Zhao Weijing[1,2], Li Yao[1,2], Dong Richang[3], Wei Rong[1,2*]

[1] *Key Laboratory for Quantum Optics, Shanghai Institute of Optics and Fine Mechanics, Chinese Academy of Sciences, Shanghai* 201800, *China*;

[2] *University of Chinese Academy of Sciences, Beijing* 100049, *China*;

[3] *Innovation Academy for Microsatellites of Chinese Academy of Sciences, Shanghai* 200120, *China*

Abstract

Objective In recent years, atomic frequency standards (AFSs) have been significantly improved and widely applied in measurement and transportation. The uncertainty of fountain AFSs has reached 10^{-16}, and that of optical AFSs is much higher at 10^{-19}, so AFSs are expected to replace Cs as a new definition of second. The development of AFSs is inseparable from the improvement of laser frequency stabilization. Narrow and ultra-narrow line-width lasers based on the frequency stabilization technology play significant roles in capturing and cooling atoms and ions, and trapping photons. Saturated absorption is widely employed in the frequency stabilization of AFSs because of its simple operation, high resolution, and the elimination of Doppler broadening. It is a technology commonly adopted in the microwave domain of atomic fountain clocks. The saturated absorption frequency stabilization of the atomic fountain clock is realized by locking a specific saturation absorption transition peak. The saturated absorption spectrum signal is modulated and demodulated to produce an error signal, and then a specific feedback signal is generated based on the error signal to control the laser output frequency. According to the output frequency, a series of modulation and frequency shifts are carried out to realize capturing, cooling, launching, and other functions which are required by the cold atom experiment. Generally, atoms have multiple saturated absorption peaks with only one involved in frequency locking, and unselected saturated absorption peaks cannot be utilized.

Methods We propose an optimized method of laser frequency stabilization based on AFSs. This method applies the frequency control in laser cooling to the frequency stabilization system and realizes the transfer locking between different saturated absorption transition peaks. The sidebands are generated by fiber electro-optic modulation. Since the zero-order diffraction light cannot meet the frequency shift requirement, the fountain system generally takes $+1$ (or -1) order diffraction light as the effective laser. We employ the -1-order diffraction light and adjust it to the maximum. Then the frequency on the saturated absorption peak of the sideband is locked to realize the laser frequency shift. A large aperture saturated absorption scheme is adopted to improve the signal-to-noise ratio (SNR) of the saturated absorption signal and its error signal after frequency shift. The feature of this scheme is to apply an adjustable aperture in the light path to improve the SNR of fringe by adjusting the size of the light spot. Finally, the signal differences in saturation absorption signals before and after modulation and optimization are compared.

Results and Discussions The probing light of the main optical path of the ^{85}Rb atomic fountain system employed for two-level detection is adopted as the light source. The 1.035 GHz wide range frequency shift is realized by an optical fiber electro-optic modulator, which meets the requirements of the transition from $|F=3\rangle \rightarrow |F'=3\rangle \otimes |F'=4\rangle$ of ^{85}Rb to $|F=2\rangle \rightarrow |F'=3\rangle$ of ^{87}Rb. $|F=3\rangle \rightarrow |F'=3\rangle \otimes |F'=4\rangle$ transition corresponds to the frequency locking position of ^{85}Rb. The energy level transfer process is shown in Fig. 2. We make the frequency-shifted laser pass through the saturated absorption optical path. Figure 4 shows the saturation absorption signal and the change of its SNR with the spot diameter. When the total input optical power remains unchanged and the spot diameter increases from 2 to 10 mm, the saturated absorption signal increases and its corresponding SNR increases by about 13 dB. Figures 4(c) and 4(d) indicate the relationship between error signal, spot diameter, and optical power. With the rising spot diameter and optical power (optical power density), the error signal and its slope increase with improved SNR. The changes in saturation absorption signal before and after modulation are shown in Fig. 5. The saturated absorption signals before and after optimization are locked respectively. The signal before the optimization is too small to lock, while the optimized signal can be locked, and the atomic cloud signal is observed in the magneto-optical trap (MOT) area as shown in Fig. 6. The locked saturated absorption signal can achieve stable operation for a long time and the error signal fluctuation is kept within 5×10^{-4} V, which meets the requirements of the atom fountain clock experiment.

Conclusions In this study, we put forward an optimized method for laser frequency stabilization. The frequency of the incident light is shifted by electro-optical modulation to realize the transfer locking of ^{85}Rb to ^{87}Rb transition peaks through the probing light from the main optical path of the ^{85}Rb fountain clock. The SNR of the transition spectral line is optimized by increasing the saturated absorption aperture, which has been improved by about 13 dB. After the frequency shift signal is locked, the atom cloud signal is observed on the atomic clock and can operate stably for a long time. By this method, we can achieve transfer locking of any frequency in the frequency range. It is also hopeful to optimize the main optical path by adding fiber electro-optical modulator (FEOM) in front of the main optical path and performing time control to realize some acousto-optic modulator (AOM) functions. As a result, the number of modulation devices is reduced and the optical path is simplified. Finally, the optical power transmission efficiency is improved to the possible realization of all fiber links.

Key words atom fountain; electro-optic modulation; frequency shift; saturated absorption; stability